


Article

Scaling Law of Flow and Heat Transfer Characteristics in Turbulent Radiative Rayleigh-Bénard Convection of Optically Thick Media [†]

Jiajun Song ¹, Panxin Li ^{1,2}, Lu Chen ^{1,3} , Yuhang Zhao ¹, Fengshi Tian ¹ and Benwen Li ^{1,*}

¹ Key Laboratory of Ocean Energy Utilization and Energy Conservation of Ministry of Education, School of Energy & Power Engineering, Dalian University of Technology, Dalian 116024, China; songjjdut@163.com (J.S.); wslpx2012@163.com (P.L.); chenluneu@163.com (L.C.); zhaoyuhang1203@163.com (Y.Z.); 13134342044@163.com (F.T.)

² Institute of Thermodynamics and Fluid Mechanics, Technische Universität Ilmenau, 98684 Ilmenau, Germany

³ MCC Capital Engineering & Research Inc., Ltd., Beijing 100176, China

* Correspondence: heatli@dlut.edu.cn

[†] Correlations for the Transport Characteristics of Radiative Rayleigh-Bénard Convection in Optically Thick Media, Shanghai, China, 12–14 August.

Abstract: Radiative natural convection is of vital importance in the process of energy storage, power generation, and thermal storage technology. As the attenuation coefficients of many heat transfer media in these fields are high enough to be considered as optically thick media, like nanofluids or molten salts in concentrated solar power or phase change thermal storage, Rosseland approximation is commonly used. In this paper, we delve into the impact of thermal radiation on the Rayleigh-Bénard (RB) convection. Theoretical analysis has been conducted by modifying the Grossmann-Lohse (GL) model. Based on turbulent dissipation theory, the corresponding scaling laws in four main regimes are proposed. Direct numerical simulation (DNS) was also performed, revealing that radiation exerts a notable influence on both flow and heat transfer, particularly on the formation of large-scale circulation. By comparing with DNS results, it is found that due to the presence of radiation, the modified Nu scaling law in small Pr range of the GL model is more suitable for predicting the transport characteristics of optical thick media with large Pr . The maximum deviation between the results of DNS and prediction model is about 10%, suggesting the summarized scaling law can effectively predict the Nu of radiative RB convection.

Keywords: solar energy; energy storage power generation; Radiative Rayleigh-Bénard convection; optically thick media; scaling law



Citation: Song, J.; Li, P.; Chen, L.; Zhao, Y.; Tian, F.; Li, B. Scaling Law of Flow and Heat Transfer Characteristics in Turbulent Radiative Rayleigh-Bénard Convection of Optically Thick Media. *Energies* **2024**, *17*, 5009. <https://doi.org/10.3390/en17195009>

Academic Editor: Artur Blaszczyk

Received: 12 September 2024

Revised: 4 October 2024

Accepted: 6 October 2024

Published: 8 October 2024



Copyright: © 2024 by the authors. Licensee MDPI, Basel, Switzerland. This article is an open access article distributed under the terms and conditions of the Creative Commons Attribution (CC BY) license (<https://creativecommons.org/licenses/by/4.0/>).

1. Introduction

The increased uptake of the renewable energy has led to an increased need for updating solar thermal energy utilization and thermal storage technology. For example, by combining concentrated solar power with photovoltaics, both the heat and electricity can be provided at the same system, making the energy maximally utilized [1]. What is more, the combined heat and power system, when paired with a phase change thermal storage system [2,3], can achieve a continuous supply of energy. Obviously, understanding and optimizing these fluid transport characteristics is essential for the development and improvement of these energy conversion and storage systems.

It is worth noting that, in applications of the above fields, the operating temperature is usually high and the temperature difference in the system may also be considerable. This makes the effect of thermal radiation non-negligible, which is a typical radiative convection problem. Different from thermal conduction and convection, the radiative energy can penetrate into the interior of the fluid, and transfer between all the elements, as it propagates as an electromagnetic wave. Besides, the directional and spectral natures of radiation

increase the dimensionality of the problem, making the determination of radiative heat flux complex. Therefore, many simplified models have been proposed, and the Rosseland diffusion approximation is the most widely used in the radiative convection of optical thick media, in which the radiative heat flux is supposed to be a function of temperature gradient, i.e., $q^R \sim -\frac{16\sigma T_{\text{ref}}^3}{3\beta_r} \frac{\partial T}{\partial x}$ (linear approximation) or $q^R \sim -\frac{16\sigma T^3}{3\beta_r} \frac{\partial T}{\partial x}$ (nonlinear approximation). For example, by using linear Rosseland approximation, Sheikholeslami et al. [4] studied the nanofluid flow and heat transfer under the effect of electric field in a porous lid driven cavity. They found thermal radiation can enhance the temperature gradient near the positive electrode, as well as the convective mode. Similar conclusions were obtained by many other researchers [5–7]. Besides, with the help of nonlinear Rosseland approximation, Shah et al. [8] proposed an artificial neural network model for heat transfer problem in carbon nanotubes-based nanofluid, which shows excellent performances by comparing with numerical simulation. Yousuf Ali et al. [9] investigated the effect of radiation on the heat transfer of nanofluids flowing through a stretching sheet by using both linear and nonlinear Rosseland approximations, and found that the thermal performance is enhanced.

Indeed, the influence of radiation on natural convection has been a subject of extensive research for many years [10–12]. Kolsi et al. [10] studied the radiative natural convection for $Ra = 10^5$ and $Pr = 13.6$, and proposed that, compared to peripheral spiraling motion, the principal flow structure is more sensitive to radiation effect. What is more, in absence of radiation there exists a zone where the flow structure exhibits quasi-2D characteristics, while the effect of radiation on the 3D behavior of the flow is significant, especially in the core of cavity. Wang et al. [13] discovered that thermal radiation can reduce the spatial spreading of the plumes but has little impact on the kinetic field. However, some other scholars suggested that the thermal radiation shows a stabilizing effect on natural convection. Both the convection and convective heat transfer are dampened by the surface radiation [14–17]. In fact, it has been observed that radiation emanating from the medium exhibits a similar dampening influence on the convective heat transfer [18,19].

The aforementioned studies hold crucial significance, but most of them have derived qualitative conclusions. In order to quantitatively determine the influence of control parameters on the transport characteristics of natural convection, some prediction models for radiative natural convection have been developed. Gad et al. [20] proposed the scaling law of heat transfer in laminar natural convection with radiation for the range of $5 \times 10^3 \leq Ra \leq 10^5$, $1 \leq \Gamma \leq 5$, $0.1 \leq \varepsilon_e \leq 0.85$. By applying k - ε turbulence model, Miroschnichenko et al. [16] investigated the heat transport characteristics for turbulent flow in a cavity, which is heated below and cooled by the environment on the other walls. They also summarized the correlations between Nu and (Ra, ε_e) for $10^9 \leq Ra \leq 10^{10}$ and $0 \leq \varepsilon_e \leq 0.6$. One of the most prominent works is the POD-based low-order model derived by Soucasse et al. [21,22] in the range of $10^6 \leq Ra \leq 10^8$, $Pr = 0.7$. Both the observed and predicted models they derived can capture the dynamics and energy transport features of the natural convection coupled with radiation. More relevant researches can be found in the review provided by Song et al. [23]. Nevertheless, one can easily see that most of the existing scaling laws are applicable within a narrow range of parameters and are insufficient to meet the needs of industrial design.

In fact, in the specific case of Rayleigh-Bénard (RB) convection, several scaling laws have been proposed, including the marginal stability theory [24], Chicago mixing zone model [25–27], Shraiman-Siggia model (SS model) [28,29], Grossmann-Lohse theory (GL model) [30–33], and so on. The GL model is widely recognized due to its wide applicability and high accuracy. Besides, it is used as a basis for many other correction models to describe the transport characteristics of RB convection under additional effects. Chakraborty [34] suggested that, by introducing the concept of magnetic energy dissipation, the arguments and assumptions in GL model can be extended to the case of turbulent magnetohydrodynamic (MHD) RB convection with a vertical magnetic field. Based on this idea, Zürner et al. [35,36] have given a set of implicit scaling equations between (Nu, Re) and (Ra, Pr, Ha) in a limited parameter range ($Pr \leq 3 \times 10^{-2}$, $Pm = \mu\sigma_b v \leq 10^{-5}$). Moreover, the

scaling behaviors of heat and momentum transport in MHD-RB convection were analyzed by Yan et al. [37] on the basis of the ratio of magnetic energy to kinetic energy and the contribution of viscous and ohmic dissipation. Therefore, analogous methodologies were adopted in this study for modeling the transport characteristics of radiative RB convection for the first time.

In this paper, a comprehensive study of the flow and heat transfer characteristics in radiative Rayleigh-Bénard convection within optically thick media has been conducted by using both theoretical analysis and direct numerical simulation. Based on the GL model, the relevant scaling laws have been derived according to the turbulent dissipation theory and the relative contribution of bulk and boundary layers to dissipation. In order to verify the prediction models, direct numerical simulation for the flow in the range of $Ra = 1 \times 10^8 \sim 5 \times 10^8$, $Pr = 7, 30$, $\mathbb{R} = 1.0 \sim 6.0$ (The definition of dimensionless parameters is depicted in Equation (6)) has also been conducted. The results show the proposed scaling law can effectively predict the Nu of radiative Rayleigh-Bénard convection, especially for situations with large optical thicknesses. The conclusions drawn from this paper can furnish a theoretical underpinning for industrial design pertaining to the realms of energy storage, power generation, and thermal storage technology.

Section 2 introduces the model and assumptions used in this theoretical analysis. Section 3 shows the scaling law in different regimes and the boundaries between them. Section 4 displays the direct numerical simulation results used to validate theoretical analysis. Finally, the conclusions of this study are presented in Section 5.

2. The Model

Before the theoretical analysis and numerical simulation, some assumptions need to be introduced first:

- An incompressible and optically thick fluid is considered;
- The Boussinesq approximation, as well as Rosseland diffusion approximation are invoked in this work;
- The flow is in a turbulent state and there exists a large-scale circulation (LSC);
- The kinetic BL is assumed to be of Prandtl-Blasius type.

Therefore, considering a fluid layer differentially heated by two rigid plates, the following governing equations can be obtained, shown as Equations (1)–(3):

$$\nabla \cdot \mathbf{u} = 0 \quad (1)$$

$$\partial_\tau \mathbf{u} + (\mathbf{u} \cdot \nabla) \mathbf{u} = -\frac{1}{\rho} \nabla p + \nu \nabla^2 \mathbf{u} + g\beta \Delta e_z \quad (2)$$

$$\partial_\tau T + \mathbf{u} \cdot \nabla T = \kappa \nabla^2 T - \frac{1}{\rho c_p} \nabla q^R \quad (3)$$

The radiative heat flux by employing Rosseland approximation is defined as Equation (4):

$$q^R = -\frac{4}{3} \frac{\sigma}{\beta_r} \nabla T^4 \quad (4)$$

When neglecting the high-order terms from the Taylor series of T^4 about T_{ref} (here the linear Rosseland approximation is considered), the radiative heat source in Equation (3) can be obtained as Equation (5):

$$\nabla q^R = -\frac{16}{3} \frac{\sigma T_{\text{ref}}^3}{\beta_r} \nabla^2 T \quad (5)$$

Here three important criterion numbers, say, the Rayleigh number Ra , Prandtl number Pr and radiation parameter \mathbb{R} , as well as two response criterion numbers, Nusselt number Nu and Reynold number Re , to characterize the RB convection, are defined as Equation (6):

$$Ra = \frac{g\beta\Delta h^3}{\nu\kappa}, Pr = \frac{\nu}{\kappa}, \mathbb{R} = 1 + \frac{4}{3} \frac{1}{\tau_r Pl}$$

$$Nu = \frac{\langle wT \rangle_A - \kappa \partial_z \langle T \rangle_A}{\kappa \Delta h^{-1}}, Re = \frac{\bar{u}h}{\nu}$$
(6)

In above equations, e_z , $\mathbf{u} = \{u, v, w\}$, $t, p, h, T, \Delta = T_h - T_c, g, \beta, \kappa, \lambda, \bar{u}, \beta_r$, and σ are the unit vector in the z direction, velocity, time, pressure, distance between two differential heated plates, temperature, temperature difference between the two plates, gravitational acceleration, thermal expansion coefficient, thermal diffusivity, thermal conductivity, the mean large-scale velocity, spectral extinction coefficient, and Stefan-Boltzmann constant ($\sigma = 5.67 \times 10^{-8} \text{W} \cdot \text{m}^{-2} \cdot \text{K}^{-4}$), respectively. The determination of characteristic quantities is illustrated in the Figure 1. Subscript h and c stand for the hot bottom and cold top plates, individually. $\tau_r = \beta_r h$ is the optical thickness. $Pl = \frac{\lambda/h}{4\sigma T_{\text{ref}}^3}$ is the Planck number. T_{ref} is the reference temperature, which will be discussed later. $\langle \cdot \rangle_A$ denotes the average over any horizontal plane (z -plane).

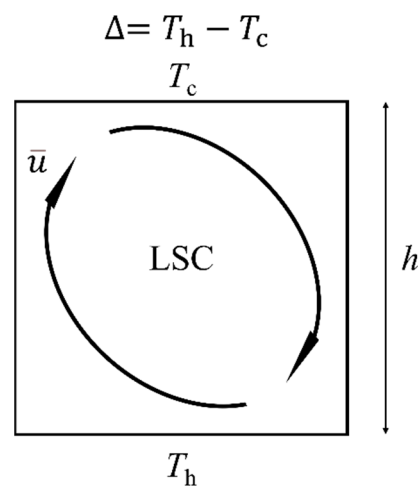


Figure 1. The dependence of characteristic quantities.

Generally, the mean temperature, $T_{m\text{-ref}} = (T_h + T_c)/2$ is usually considered as the reference temperature. However, due to the dependence of radiative heat transfer on $|T_h^4 - T_c^4|$, another strategy has been proposed [38] as Equation (7):

$$T_{\text{rad-ref}} = \left(\frac{T_h^4 + T_c^4}{2} \right)^{\frac{1}{4}}$$
(7)

By comparing these two reference temperatures, the relative error between them can be gained, shown as Equation (8):

$$O = \frac{T_{\text{rad-ref}} - T_{m\text{-ref}}}{T_{m\text{-ref}}} = \left[8 \cdot \frac{1 + (T_h/T_c)^4}{(1 + T_h/T_c)^4} \right]^{\frac{1}{4}} - 1$$
(8)

Figure 2 depicts the dependence of the temperature difference (Δ and Δ/T_c) and O upon T_c . It can be easily seen that even if the relative temperature difference Δ/T_c reaches 50%, O is only 5.56%. It should be noticed that the basic premise for applying the Boussinesq approximation is that the physical properties of fluid do not change significantly except for the density. As shown in Figure 1, Δ has exceeded 100 K for $T_c > 200$ K and $\Delta/T_c = 50\%$. Indeed, such a large temperature difference usually leads to significant changes in the physical properties of fluid. Under such conditions, the Boussinesq approximation is no longer valid. Therefore, either of these two reference temperatures can usually be considered for most cases with small temperature differences.

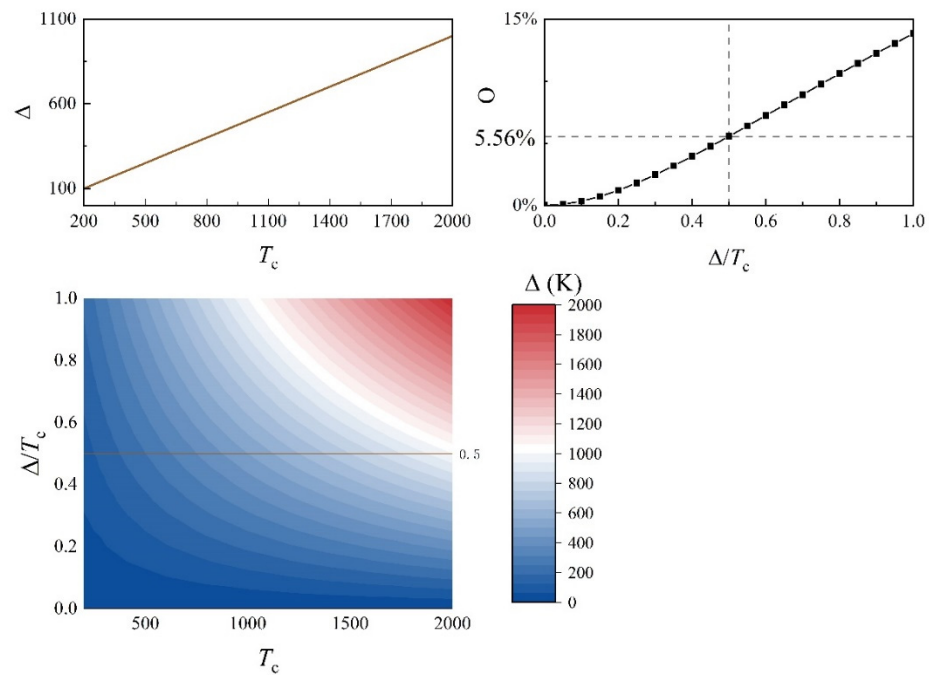


Figure 2. The dependence of the temperature difference (Δ and Δ/T_c) and O upon T_c .

3. Scaling Laws

In correspondence with classical RB convection, one can derive the following rigorous relations for the global averaged kinetic and thermal dissipation rates, ϵ_u and ϵ_T , according to the theory of Shraiman and Siggia [28,29], as shown in Equations (9) and (10):

$$\epsilon_u = \langle \epsilon_u(x, t) \rangle_V = \frac{\nu^3}{h^4} (Nu - 1) Ra Pr^{-2} \tag{9}$$

$$\epsilon_T = \langle \epsilon_T(x, t) \rangle_V = \kappa \frac{\Delta^2}{h^2} Nu \tag{10}$$

where $\langle \cdot \rangle_V$ denotes the volume average. $\epsilon_u(x, t) = \nu [\partial_i u_j(x, t)]^2$ and $\epsilon_T(x, t) = \kappa [\partial_i T_j(x, t)]^2$ are the local kinetic and thermal dissipation rates.

The main idea of Grossmann-Lohse theory [30–33] is that the global averaged energy dissipations can be decomposed into the bulk and boundary layer (BL) contributions, as shown in Equation (11):

$$\epsilon = \epsilon_{\text{bulk}} + \epsilon_{\text{BL}} \tag{11}$$

By means of dimensional analysis, the different contributions can be estimated as Equations (12)–(17):

$$\epsilon_{u\text{-bulk}} \sim \frac{\bar{u}^3}{h} = \frac{\nu^3}{h^4} Re^3 \tag{12}$$

$$\epsilon_{T\text{-bulk}} \sim \frac{\bar{u} \Delta^2}{h} = \kappa \frac{\Delta^2}{h^2} Pr Re \text{ (for } \frac{\delta_u}{\delta_T} < 1) \tag{13}$$

$$\epsilon_{T\text{-bulk}} \sim \bar{u} \frac{\delta_T}{\delta_u} \frac{\Delta^2}{h} = \kappa \frac{\Delta^2}{h^2} \mathbb{R} Pr Re^{\frac{3}{2}} Nu^{-1} \text{ (for } \frac{\delta_u}{\delta_T} > 1) \tag{14}$$

$$\epsilon_{u\text{-BL}} \sim \nu \frac{\bar{u}^2}{\delta_u^2} \frac{\delta_u}{h} \sim \frac{\nu^3}{h^4} Re^{\frac{5}{2}} \tag{15}$$

$$\epsilon_{T\text{-BL}} \sim \kappa \frac{\Delta^2}{\delta_T^2} \frac{\delta_T}{h} \sim \kappa \frac{\Delta^2}{h^2} \mathbb{R}^{\frac{1}{2}} Pr^{\frac{1}{2}} Re^{\frac{1}{2}} \text{ (for } \frac{\delta_u}{\delta_T} < 1) \tag{16}$$

$$\varepsilon_{T-BL} \sim \kappa \frac{\Delta^2}{\delta_T^2} \frac{\delta_T}{h} \sim \kappa \frac{\Delta^2}{h^2} \mathbb{R}^{\frac{2}{3}} Pr^{\frac{1}{3}} Re^{\frac{1}{2}} \left(\text{for } \frac{\delta_u}{\delta_T} > 1\right) \tag{17}$$

where $\delta_u \sim hRe^{-\frac{1}{2}}$ and $\delta_T \sim \mathbb{R}hNu^{-1}$ are the thickness of the kinetic and thermal BL, respectively. Their ratio is related to Pr , i.e., $Pr \sim \delta_u/\delta_T$. It should be emphasized that the kinetic BL is assumed to be of Prandtl-Blasius type in Grossmann-Lohse theory.

Utilizing the aforementioned relations, four main regimes can be easily identified as shown in Table 1, contingent upon whether the bulk or BL is the primary contributor to energy dissipation:

Table 1. The four main regimes and the primary contributors.

	ε_u	ε_T
Regime I	ε_{u-BL}	ε_{T-BL}
Regime II	ε_{u-bulk}	ε_{T-BL}
Regime III	ε_{u-BL}	ε_{T-bulk}
Regime IV	ε_{u-bulk}	ε_{T-bulk}

Additionally, based on the relative thickness of the kinetic and thermal BL, each main regime can be divided into two sub-regions, i.e., $\delta_u/\delta_T < 1$ or $\delta_u/\delta_T > 1$. The scaling laws are given in each sub-region as following:

- *Regime I-a:* $\varepsilon_u \sim \varepsilon_{u-BL}$, $\varepsilon_T \sim \varepsilon_{T-BL}$, $\delta_u/\delta_T < 1$

Substituting Equations (8) and (9) into Equations (15) and (16), respectively, one can get the following equations as shown in Equations (18) and (19):

$$Re = \mathbb{R}^{\frac{1}{4}} Ra^{\frac{1}{2}} Pr^{-\frac{3}{4}} \tag{18}$$

$$Nu = \mathbb{R}^{\frac{5}{8}} Ra^{\frac{1}{4}} Pr^{\frac{1}{8}} \tag{19}$$

- *Regime I-b:* $\varepsilon_u \sim \varepsilon_{u-BL}$, $\varepsilon_T \sim \varepsilon_{T-BL}$, $\delta_u/\delta_T > 1$

By combining Equations (8) with (15) and (9) with (17), the following relations can be obtained as shown in Equations (20) and (21):

$$Re = \mathbb{R}^{\frac{1}{3}} Ra^{\frac{1}{2}} Pr^{-\frac{5}{6}} \tag{20}$$

$$Nu = \mathbb{R}^{\frac{5}{6}} Ra^{\frac{1}{4}} Pr^{-\frac{1}{12}} \tag{21}$$

- *Regime II-a:* $\varepsilon_u \sim \varepsilon_{u-bulk}$, $\varepsilon_T \sim \varepsilon_{T-BL}$, $\delta_u/\delta_T < 1$

Using Equations (8), (9), (12) and (16), one can obtain the following equations as shown in Equations (22) and (23):

$$Re = \mathbb{R}^{\frac{1}{5}} Ra^{\frac{2}{5}} Pr^{-\frac{3}{5}} \tag{22}$$

$$Nu = \mathbb{R}^{\frac{3}{5}} Ra^{\frac{1}{5}} Pr^{\frac{1}{5}} \tag{23}$$

- *Regime II-b:* $\varepsilon_u \sim \varepsilon_{u-bulk}$, $\varepsilon_T \sim \varepsilon_{T-BL}$, $\delta_u/\delta_T > 1$

Using Equation (17) instead of (16) for (9), we can get the following equations as shown in Equations (24) and (25):

$$Re = \mathbb{R}^{\frac{4}{15}} Ra^{\frac{2}{5}} Pr^{-\frac{2}{3}} \tag{24}$$

$$Nu = \mathbb{R}^{\frac{4}{5}} Ra^{\frac{1}{5}} \tag{25}$$

- *Regime III-a:* $\varepsilon_u \sim \varepsilon_{u-BL}$, $\varepsilon_T \sim \varepsilon_{T-bulk}$, $\delta_u/\delta_T < 1$

Combining Equations (8), (9), (15) and (13), one can derive the following relations as shown in Equations (26) and (27):

$$Re = Ra^{\frac{2}{3}} Pr^{-\frac{2}{3}} \quad (26)$$

$$Nu = Ra^{\frac{2}{3}} Pr^{\frac{1}{3}} \quad (27)$$

- *Regime III-b:* $\varepsilon_u \sim \varepsilon_{u-BL}$, $\varepsilon_T \sim \varepsilon_{T-bulk}$, $\delta_u/\delta_T > 1$

Similarly, using Equation (14) instead of (13) for (9), the following relations can be obtained as shown in Equations (28) and (29):

$$Re = \mathbb{R}^{\frac{2}{7}} Ra^{\frac{4}{7}} Pr^{-\frac{6}{7}} \quad (28)$$

$$Nu = \mathbb{R}^{\frac{5}{7}} Ra^{\frac{3}{7}} Pr^{-\frac{1}{7}} \quad (29)$$

- *Regime IV-a:* $\varepsilon_u \sim \varepsilon_{u-bulk}$, $\varepsilon_T \sim \varepsilon_{T-bulk}$, $\delta_u/\delta_T < 1$

Substituting Equations (12) and (13) into Equations (8) and (9), respectively, one can get the following relations as shown in Equations (30) and (31):

$$Re = Ra^{\frac{1}{2}} Pr^{-\frac{1}{2}} \quad (30)$$

$$Nu = Ra^{\frac{1}{2}} Pr^{\frac{1}{2}} \quad (31)$$

- *Regime IV-b:* $\varepsilon_u \sim \varepsilon_{u-bulk}$, $\varepsilon_T \sim \varepsilon_{T-bulk}$, $\delta_u/\delta_T > 1$

Combining Equations (8), (9), (12) and (14), the following relations can be determined as shown in Equations (32) and (33):

$$Re = \mathbb{R}^{\frac{2}{9}} Ra^{\frac{4}{9}} Pr^{-\frac{2}{3}} \quad (32)$$

$$Nu = \mathbb{R}^{\frac{2}{3}} Ra^{\frac{1}{3}} \quad (33)$$

The boundaries between the two different regimes or sub-regions can be derived by considering $\varepsilon_{bulk} \sim \varepsilon_{BL}$ or $\delta_u \sim \delta_T$, respectively. Thereby, the following correlations can be obtained as shown in Equations (34)–(43):

$$Ra_{1a-2a} \sim \mathbb{R}^{-\frac{1}{2}} Pr_{1a-2a}^{\frac{3}{2}} \quad (34)$$

$$Ra_{1a-3a} \sim \mathbb{R}^{\frac{3}{2}} Pr_{1a-3a}^{-\frac{1}{2}} \quad (35)$$

$$Ra_{3a-4a} \sim \mathbb{R}^0 Pr_{3a-4a}^1 \quad (36)$$

$$Ra_{2a-4a} \sim \mathbb{R}^2 Pr_{2a-4a}^{-1} \quad (37)$$

$$Ra_{1b-3b} \sim \mathbb{R}^{\frac{2}{3}} Pr_{1b-3b}^{\frac{1}{3}} \quad (38)$$

$$Ra_{3b-4b} \sim \mathbb{R}^{-\frac{1}{2}} Pr_{3b-4b}^{\frac{3}{2}} \quad (39)$$

$$Pr_{1a-b} \sim \mathbb{R}^1 Ra^0 \quad (40)$$

$$Pr_{2a-b} \sim \mathbb{R}^1 Ra^0 \quad (41)$$

$$Pr_{3a-b} \sim \mathbb{R}^{\frac{3}{2}} Ra^{-\frac{1}{2}} \quad (42)$$

$$Pr_{4a-b} \sim \mathbb{R}^{\frac{4}{3}} Ra^{-\frac{1}{3}} \quad (43)$$

It should be noticed that the specific correlations for the boundaries require a massive amount of experimental or simulated results, which is currently lacking. As a result, it is recommended to refer to the original model at present. What is more, one can easily see that the effect of aspect ratio, Γ , is not shown in the above scaling laws. This is due to the

fact that no significant dependence of the scaling exponent on the aspect ratio is anticipated, in contrast to the pre-factors [30,39].

4. Direct Numerical Simulations

In order to verify the above scaling laws derived from theoretical analysis, direct numerical simulation (DNS) has been conducted at the range of $Pr = (7, 30)$, $Ra = (1, 3, 5) \times 10^8$, $\mathbb{R} = 1.0 \sim 6.0$, which are common ranges of fluid parameters in practical applications [40]. The effect of thermal radiation on flow structure and heat transfer has been analyzed.

It should be noticed that $\mathbb{R} = 1.0$ stands for the case without considering radiation effects, while $\mathbb{R} = 6.0$ does not represent the limit case. Actually, according to Equation (7) and the research of Zhang et al. [41,42], the radiation parameter \mathbb{R} depends on the reference temperature, characteristic length of cavity, and attenuation coefficient of salt.

4.1. Numerical Model

The convection cell adopted in this paper is a 2D square cavity with length h and aspect ratio $\Gamma = 1$, as shown in Figure 3. The temperatures of the top and bottom walls are fixed at T_c and T_h . The sidewalls are taken to be perfectly adiabatic. No-slip velocity boundary conditions are considered for all the walls. By setting the length h , free-fall velocity $u_f = \sqrt{g\beta\Delta h}$, and temperature difference Δ to the corresponding reference scales, the following dimensionless variables can be obtained, shown as Equation (44).

$$\begin{aligned} \{X, Y, Z\} &= \frac{\{x, y, z\}}{h}, \mathbf{U} = \frac{\mathbf{u}}{u_f}, \tau = \frac{t}{h/u_f}, P = \frac{p}{\rho u_f^2} \\ \theta &= \frac{T - T_{\text{ref}}}{\Delta}, \widetilde{q}^R = -\frac{16}{3} \frac{\sigma T_{\text{ref}}^3}{\beta_r \lambda} \sqrt{\frac{1}{RaPr}} \nabla \theta \end{aligned} \tag{44}$$

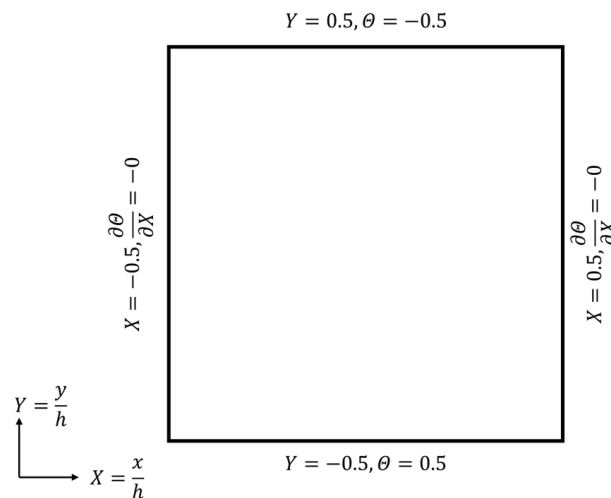


Figure 3. The convection cell and dimensionless boundary conditions.

Therefore, the dimensionless governing equations can be conventionally obtained as shown in Equations (45)–(47) (refer to Equations (1)–(3)).

$$\nabla \cdot \mathbf{U} = 0 \tag{45}$$

$$\partial_\tau \mathbf{U} + (\mathbf{U} \cdot \nabla) \mathbf{U} = -\nabla P + \sqrt{\frac{Pr}{Ra}} \nabla^2 \mathbf{U} + \theta e_z \tag{46}$$

$$\partial_\tau \theta + \mathbf{U} \cdot \nabla \theta = \sqrt{\frac{1}{RaPr}} \nabla^2 \theta - \nabla \cdot \widetilde{q}^R \tag{47}$$

where \mathbf{U} , P , θ and \widetilde{q}^R are the dimensionless velocity, pressure, temperature, and radiative heat flux, respectively.

The dimensionless boundary conditions are as shown in Equation (48):

$$\begin{aligned} X = \pm 0.5 \quad -\frac{\partial \theta}{\partial X} &= 0 \\ Y = -0.5 \quad \theta &= 0.5 \\ Y = 0.5 \quad \theta &= -0.5 \end{aligned} \quad (48)$$

The initial conditions are set to $\tau = 0$, $U = 0$, $\theta = 0$ (for fluid and sidewall), $P = 1$. In order to strike the balance between capturing system dynamics accurately and maintaining computational efficiency, the size of the time step is set to be adjustable, and the corresponding maximum Courant number is limited to 0.9. The temporal average is performed over a duration of more than 5000 dimensionless time units after the convective flow has been fully developed, to allow for the averaging out of transient fluctuations.

4.2. Numerical Method and Validation

The governing equations are discretized by adopting the finite volume method. The pressure-velocity coupling is handled by the PISO algorithm. The Crank-Nicolson scheme is used for the transient terms, the second order upwind scheme is applied to treat the convective terms, and the second order central difference scheme is adopted for diffusion terms.

As shown in Figure 4, non-equidistant meshes are applied and the computational meshes are refined close to all the four walls so that the transport characteristics in BLs can be captured. The grid independence test is carried out at $Ra = 5 \times 10^8$, $Pr = 1$. The average Nusselt numbers for different grids have been displayed in Table 2. It turns out that the solution becomes independent of grid size for 256×256 , since the deviation is less than 0.5%.

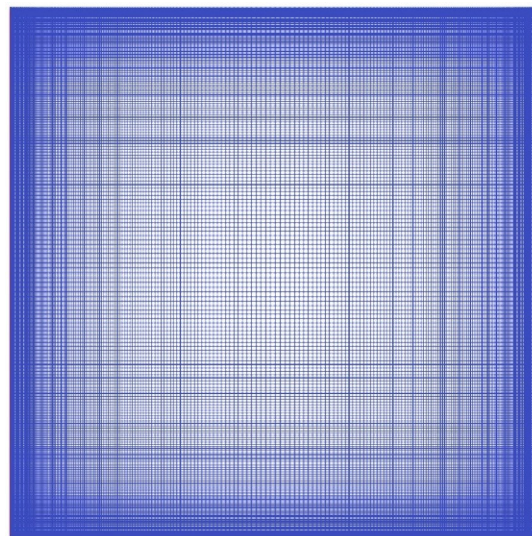


Figure 4. The sketch of grids with refined meshes near walls.

Table 2. The averaged Nusselt numbers for different grids.

Grid Size	Nu	Error (%)
128×128	39.17710	-
256×256	39.84992	1.72%
384×384	40.03957	0.48%

In order to validate the present code, the results for $Ra = 1.0 \times 10^8$, $Pr = 4.3$ were compared with those in References [43,44], as shown in Table 3. It can be seen that the maximum relative error for Nu is less than 3.5%. Therefore, the correctness of present numerical method code is verified.

Table 3. Comparisons with public results from References.

	Nu	Error (%)
Present	24.9	-
Huang et al. [43]	25.38	1.89%
Yang et al. [44]	258.0	3.49%

4.3. Effect of Radiation on Flow Structure

Figure 5 shows the time-evolution of isotherm contours (background) and streamlines (blue lines) at different \mathbb{R} when $Pr = 7, 30$ and $Ra = (1, 5) \times 10^8$. It can be seen that the large-scale circulation (LSC) has been formed when the effect of radiation is not taken into account ($\mathbb{R} = 1.0$) or weak ($\mathbb{R} = 1.8$). The shape of LSC is approximately elliptical, which follows the diagonal of the cavity as the major axis and is accompanied by two small vortices in the short axis direction. The two small vortices may expand, causing the large-scale circulation to gradually collapse and change its tilt direction. Interestingly, with the increasing \mathbb{R} , the collapse and redirection frequencies of LSC decrease. However, for the case of $\mathbb{R} = 6.0$, there are two small vortices arranged vertically. This makes it difficult for heat to exchange between the cold fluid at the top and the hot fluid at the bottom. The flow structure is similar to that of small Ra , indicating that thermal radiation suppresses flow.

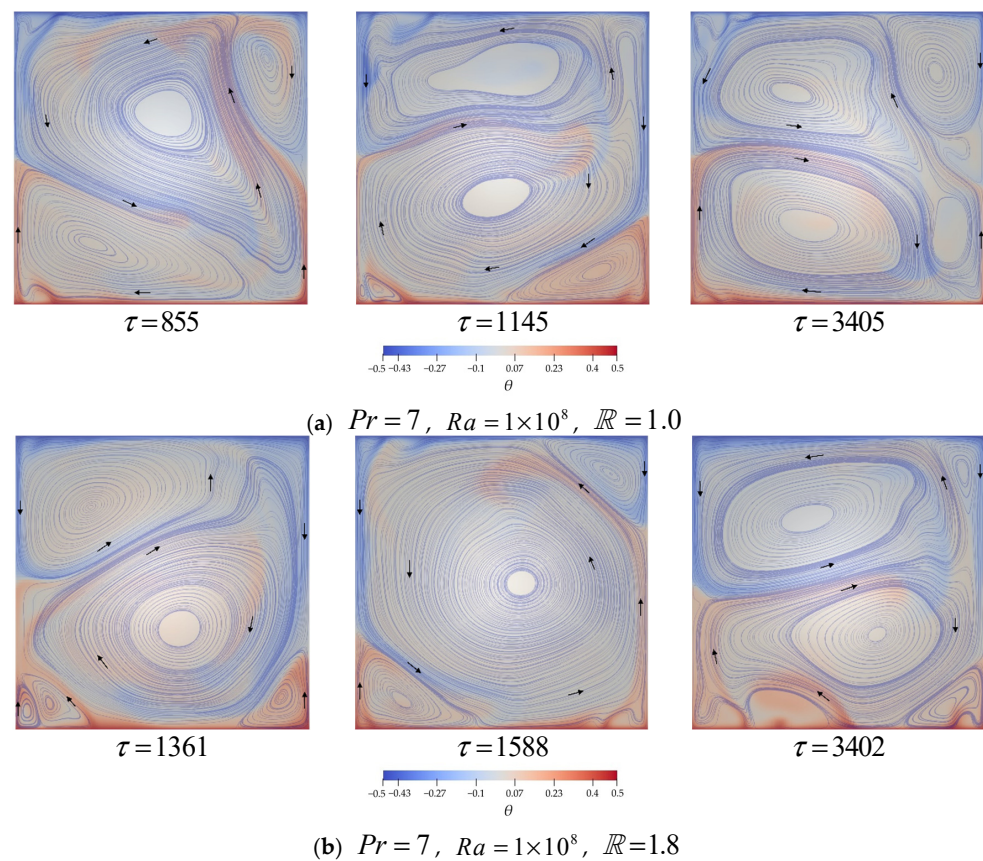
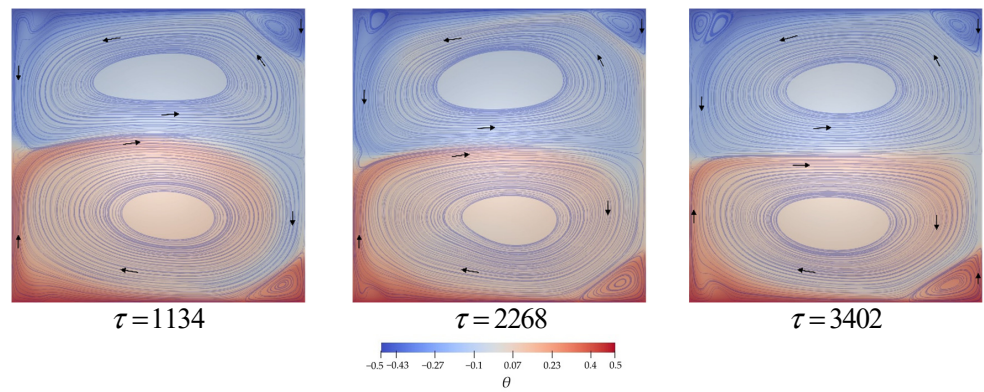
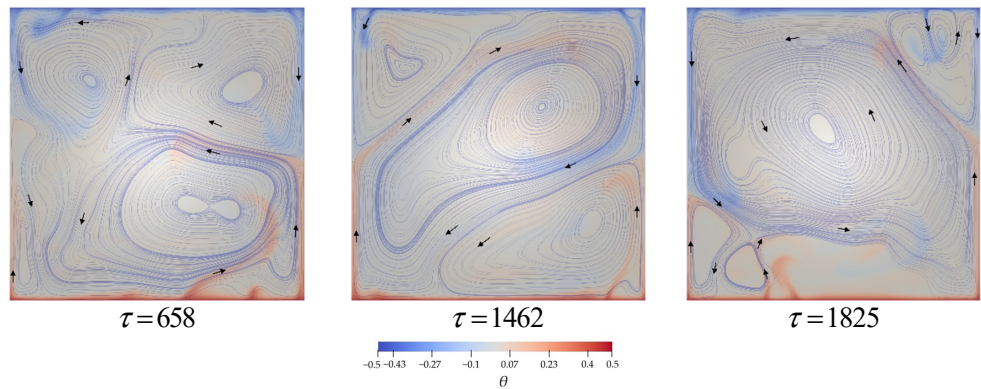


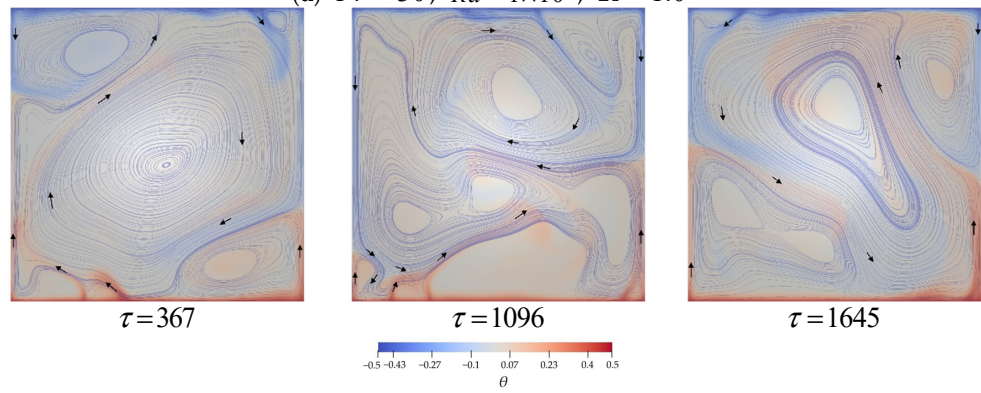
Figure 5. Cont.



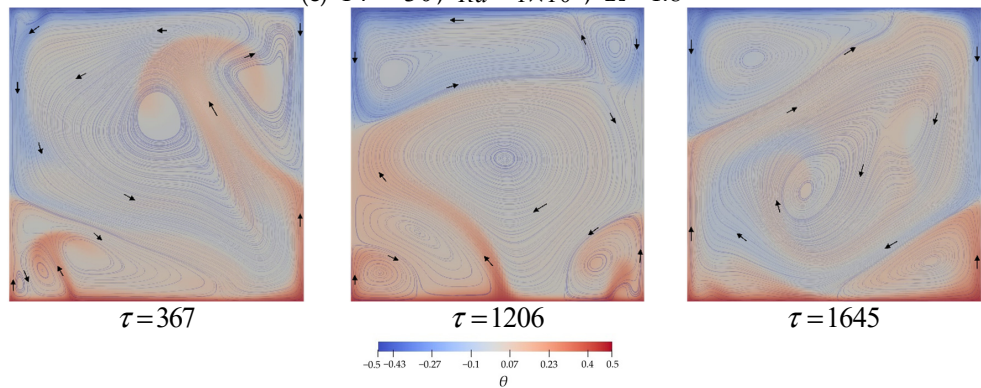
(c) $Pr = 7, Ra = 1 \times 10^8, \mathcal{R} = 6.0$



(d) $Pr = 30, Ra = 1 \times 10^8, \mathcal{R} = 1.0$



(e) $Pr = 30, Ra = 1 \times 10^8, \mathcal{R} = 1.8$



(f) $Pr = 30, Ra = 1 \times 10^8, \mathcal{R} = 6.0$

Figure 5. Cont.

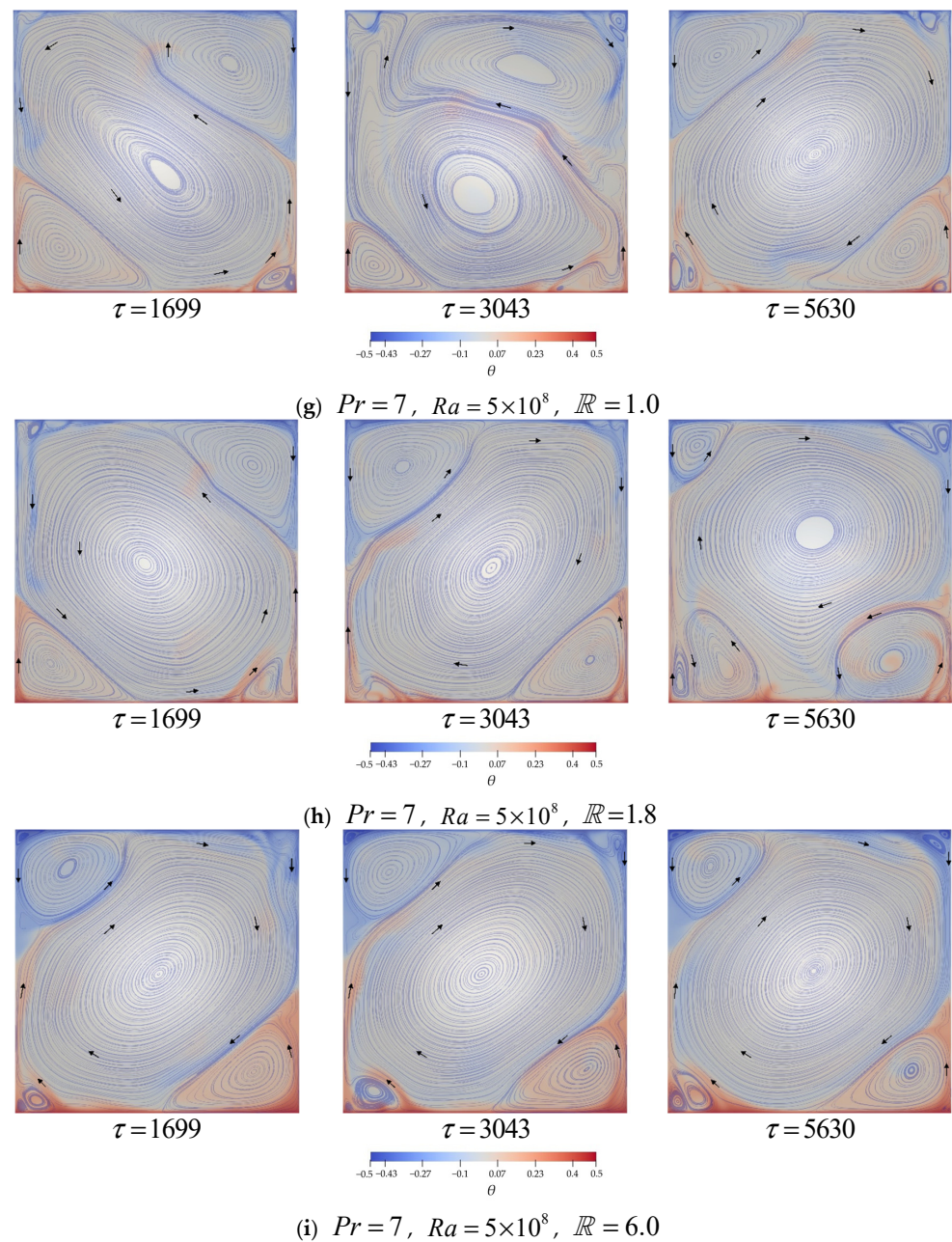


Figure 5. The time-evolution of isotherm contours (background) and streamlines (blue lines) for $Ra = (1, 5) \times 10^8, Pr = 7, 30$ at different \mathbb{R} . The direction of flow is indicated by the black arrows.

When Pr increases to 30, LSC still exists even at $\mathbb{R} = 6.0$, suggesting that the effect of thermal radiation weakens for larger Pr . Moreover, as Ra increases, the effect of thermal radiation is not sufficient to suppress the formation of LSC, but its stabilizing effect will cause a decrease in the redirection frequency of LSC.

4.4. Comparisons between Scaling Law and DNS Results

In order to quantitatively verify the correctness of Equations (19) and (21) for examples, the comparison of time average Nu between DNS results and the theoretical analysis has been performed, as shown in Figure 6. Consistent with the results of many other literatures, the heat transfer is significantly enhanced with an increase in \mathbb{R} .

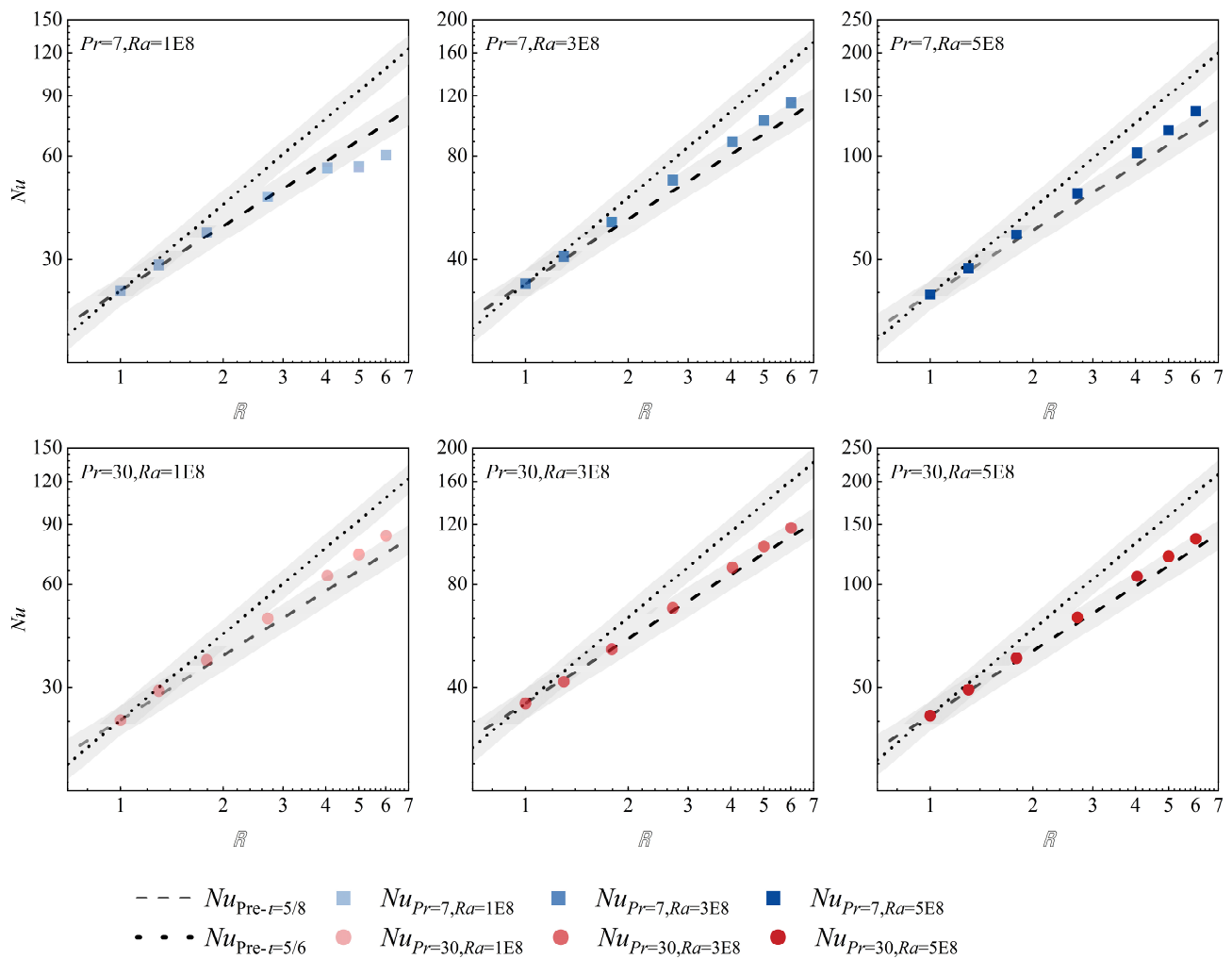


Figure 6. The comparison between DNS and prediction model: Nu . (The grey area represents a relative error of 10%).

According to the boundary division between the various regimes in the GL model [30–33], the parameter range in this paper is located in Regime I-b, where the exponent ι of \mathbb{R} in the relation $Nu \sim \mathbb{R}^\iota Ra^\alpha Pr^\gamma$ is 5/6. However, as shown in Figure 6, the relative error between simulation results and the predicted results of the relation $Nu \sim \mathbb{R}^{5/8}$ in Regime I-a is relatively small (about 10%). This phenomenon may be attributed to the increase of δ_T , which arises due to the suppression of convection by thermal radiation and the increase in fluid temperature uniformity. Actually, the increase in BL thickness was also observed by Hossain et al. [45].

Figure 7 depicts the exponent ι of \mathbb{R} obtained from theoretical analysis and DNS. It can be seen that the deviation in between is about 10%. Besides, the deviation decreases with the increase of Pr and Ra . Similar conclusions for the range of $Pr = 1$ (usually gas) and $Ra = (3 \sim 4) \times 10^8$ can be obtained in our previous work [46]. Both of them indicate that the derived scaling law can effectively predict the Nu of radiative Rayleigh-Bénard convection by applying the Rosseland approximation.

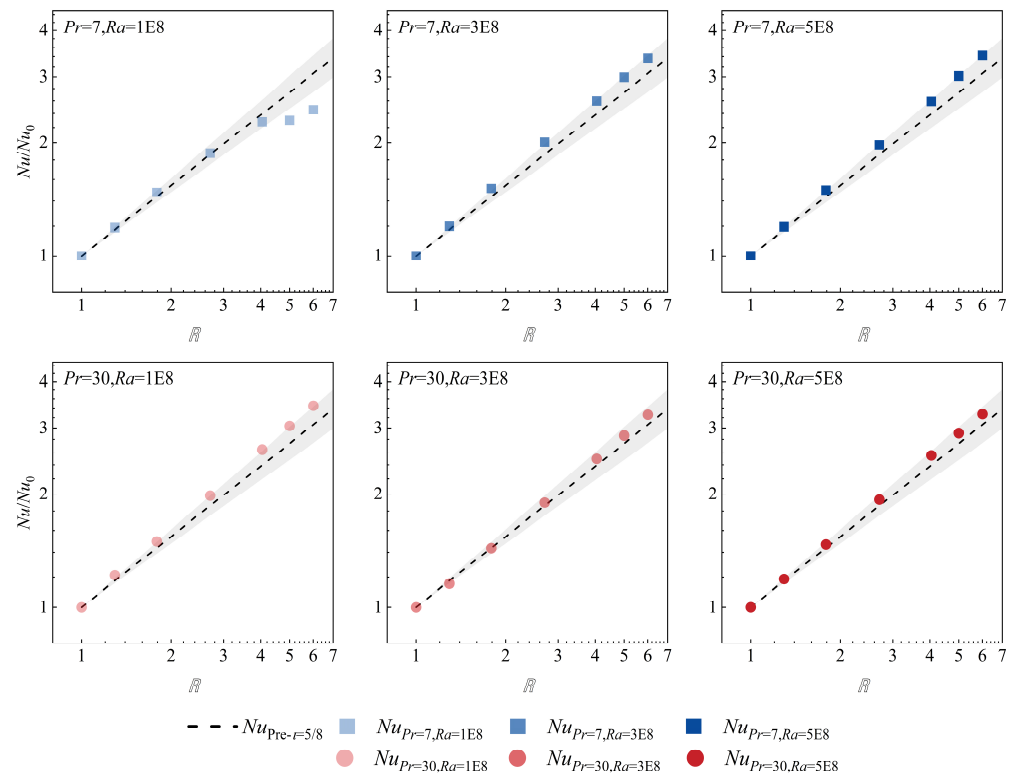


Figure 7. The comparison between DNS and prediction model: the exponent ι of \mathbb{R} . (The grey area represents a relative error of 10%).

5. Conclusions

In summary, the transport characteristics of radiative Rayleigh-Bénard convection in optically thick media with large Pr have been investigated by both theoretical analysis and DNS. Main conclusions can be summarized as follows:

- (1) Based on the turbulent dissipation theory and Rosseland approximation, the scaling laws in the four main regimes have been summarized within the scope of numerical simulation research presented in this paper ($Pr = (7, 30)$, $Ra = (1, 3, 5) \times 10^8$, $\mathbb{R} = 1.0 \sim 6.0$), $Nu = \mathbb{R}^{\frac{5}{8}} Ra^{\frac{1}{4}} Pr^{\frac{1}{8}}$.
- (2) It has been found that due to the presence of thermal radiation, the Nu scaling law in the small Pr range of the GL model is more suitable for predicting the transport characteristics of optical thick media with large Pr . The deviation between the results of DNS and prediction model is approximately 10%.
- (3) The determination of reference temperature is discussed, and there is almost no difference between the arithmetic mean temperature and radiative mean temperature, especially within the scope of application of Boussinesq approximation.
- (4) The influence of thermal radiation results in a significant enhancement of heat transfer.
- (5) When $Ra > 1 \times 10^8$, the LSC can be formed for weak radiation effect. The effect of radiation can stabilize flow, specifically manifested by a collapse of LSC as \mathbb{R} increases. However, the radiation effect weakens for larger Pr .

These conclusions offer a theoretical underpinning for industrial designs related to energy storage, power generation, and thermal storage technology. Future research endeavors can focus on determining the pre-factors of scaling laws to further refine and enhance our understanding of these processes.

Author Contributions: Conceptualization, J.S.; methodology, J.S.; software, J.S., P.L. and L.C.; validation, J.S., Y.Z. and F.T.; formal analysis, J.S.; investigation, J.S.; resources, B.L.; data curation, J.S.; writing—original draft preparation, J.S.; writing—review and editing, J.S., P.L., L.C., Y.Z., F.T. and B.L.; visualization, J.S.; supervision, J.S. and B.L.; project administration, J.S. and B.L.; funding acquisition, J.S. and B.L. All authors have read and agreed to the published version of the manuscript.

Funding: This research was funded by the Central Guiding Local Science and Technology Development Fund Projects (No. 2023JH6/100100020), Liaoning Province International Science and Technology Cooperation Plan (No. 2023JH2/10700001), Dalian Science and Technology Plan Project (No. 2023JJ12SN028) and the Natural Science Foundation of China (No. 51976021).

Data Availability Statement: The data presented in this study are available on request from the corresponding author, since the data are not publicly available due to privacy and ethical restrictions.

Conflicts of Interest: Author Lu Chen was employed by the company, MCC Capital Engineering & Research Inc., Ltd. The remaining authors declare that the research was conducted in the absence of any commercial or financial relationships that could be construed as a potential conflict of interest.

Nomenclature

g	gravitational acceleration	$\text{m}\cdot\text{s}^{-2}$
h	length of the cavity	m
Ha	Hartmann number	-
I, I_b	radiation intensity, radiation intensity of black body	$\text{W}\cdot\text{m}^{-2}$
Nu	Nusselt number	-
p, P	pressure, dimensionless pressure	$\text{kg}\cdot\text{m}^{-1}\cdot\text{s}^{-1}, -$
Pl	Planck number	-
Pr	Prandtl number	-
q^R	radiative heat flux	$\text{W}\cdot\text{m}^{-2}$
Ra	Rayleigh number	-
Re	Reynold number	-
s	position vector	m
t	time	s
T	temperature	K
T_{ref}	reference temperature	K
$u = \{u, v, w\}$	velocity	$\text{m}\cdot\text{s}^{-1}$
\mathbf{u}	dimensionless velocity vector	-
u_f	free-fall velocity	$\text{m}\cdot\text{s}^{-1}$
\bar{u}	the mean large-scale velocity	$\text{m}\cdot\text{s}^{-1}$
x, y, z	Cartesian coordinates	m
\mathbb{R}	radiation parameter	-
$\langle \cdot \rangle_A$	the average over any horizontal plane	-
$\langle \cdot \rangle_V$	the volume average	-
Δ	temperature difference	K
Greek symbols		
β	thermal expansion coefficient	K^{-1}
β_r	spectral extinction or attenuation coefficient	m^{-1}
Γ	aspect ratio	-
δ	the thickness of BL	m
ε	energy dissipation	-
ε_e	emissivity	-
θ	dimensionless temperature	-
κ	thermal diffusivity	$\text{m}^2\cdot\text{s}^{-1}$
$\kappa_{a,\lambda}$	scattering coefficient	m^{-1}
λ	thermal conductivity	$\text{W}\cdot\text{m}^{-1}\cdot\text{K}^{-1}$
σ	Stefan-Boltzmann constant	$\sigma = 5.67 \times 10^{-8} \text{W} \cdot \text{m}^{-2} \cdot \text{K}^{-4}$
$\sigma_{s,\lambda}$	absorption coefficient	m^{-1}
τ	dimensionless time	-

τ_r	optical thickness	-
ν	kinematic viscosity	$\text{m}^2 \cdot \text{s}^{-1}$
Φ	scattering phase function	-
Ω, Ω'	solid angle, incident solid angle	sr
Subscripts		
h	hot plate	
c	cold plate	
u	kinetic related quantities	
T	thermal related quantities	
BL	contribution from BL	
bulk	contribution from bulk	
λ	spectrally dependent	

References

1. Arnautakis, G.E.; Katsaprakakis, D.A. Energy yield of spectral splitting concentrated solar power photovoltaic systems. *Energies* **2024**, *17*, 556. [\[CrossRef\]](#)
2. Zhou, W.; Yang, Z.; Lin, L.; Feng, Y. Molecular insights into thermal conductivity enhancement and interfacial heat transfer of molten salt/porous ceramic skeleton composite phase change materials. *Int. J. Heat Mass Transf.* **2024**, *232*, 125934. [\[CrossRef\]](#)
3. Yuan, H.M.; Liu, S.T.; Li, T.H.; Yang, L.Y.; Li, D.H.; Bai, H.; Wang, X.D. Review on thermal properties with influence factors of solid-liquid organic phase-change micro/nanocapsules. *Energies* **2024**, *17*, 604. [\[CrossRef\]](#)
4. Sheikholeslami, M.; Rokni, H.B. Numerical simulation for impact of Coulomb force on nanofluid heat transfer in a porous enclosure in presence of thermal radiation. *Int. J. Heat Mass Transf.* **2018**, *118*, 823–831. [\[CrossRef\]](#)
5. Qasem, S.A.; Sivasankaran, S.; Siri, Z.; Mothman, W.A. Effect of thermal radiation on natural convection of a nanofluid in a square cavity with a solid body. *Therm. Sci.* **2021**, *25*, 1949–1961. [\[CrossRef\]](#)
6. Alnaqi, A.A.; Aghakhani, S.; Pordanjani, A.H.; Bakhtiari, R.; Asadi, A.; Minh-Duc, T. Effects of magnetic field on the convective heat transfer rate and entropy generation of a nanofluid in an inclined square cavity equipped with a conductor fin: Considering the radiation effect. *Int. J. Heat Mass Transf.* **2019**, *133*, 256–267. [\[CrossRef\]](#)
7. Roy, N.C.; Saha, L.K.; Siddiq, S. Electrohydrodynamics and thermal radiation effects on natural convection flow in an enclosed domain. *Int. Commun. Heat Mass Transf.* **2021**, *126*, 105437. [\[CrossRef\]](#)
8. Shah, F.; Asadullah; Ali, S.; Khan, S.U.; Akermi, M.; Nasr, S.; Hassani, R.; Jaballah, N.S. Thermal analysis for SWCNTs and MWNTs due to coaxially stretchable disks with applications of viscous dissipation and thermal radiation: Artificial neural network analysis. *Int. Commun. Heat Mass Transf.* **2024**, *155*, 107452. [\[CrossRef\]](#)
9. Ali, M.Y.; Rahman, M.; Ali, M.M.; Ahmmed, S.F.; Haque, S. Data analysis of non-linear radiative electro-periodic MHD flow past a stretching sheet with activation energy impact. *Int. Commun. Heat Mass Transf.* **2024**, *155*, 107572.
10. Kolsi, L.; Abidi, A.; Maatki, C.; Borjini, N.M.; Aissia, B.H. Combined radiation-natural convection in three-dimensional verticals cavities. *Therm. Sci.* **2011**, *15*, S327–S339. [\[CrossRef\]](#)
11. Leporini, M.; Corvaro, F.; Marchetti, B.; Polonara, F.; Benucci, M. Experimental and numerical investigation of natural convection in tilted square cavity filled with air. *Exp. Therm. Fluid Sci.* **2018**, *99*, 572–583. [\[CrossRef\]](#)
12. El Ayachi, R.; Raji, A.; Hasnaoui, M.; Bahlaoui, A. Combined effect of radiation and natural convection in a square cavity differentially heated with a periodic temperature. *Numer. Heat Transf. Part A-Appl.* **2008**, *53*, 1339–1356. [\[CrossRef\]](#)
13. Wang, Y.; Sergent, A.; Saury, D.; Lemonnier, D.; Joubert, P. Numerical study of an unsteady confined thermal plume under the influence of gas radiation. *Int. J. Therm. Sci.* **2020**, *156*, 106474. [\[CrossRef\]](#)
14. Martyushev, S.G.; Sheremet, M.A. Conjugate natural convection combined with surface thermal radiation in a three-dimensional enclosure with a heat source. *Int. J. Heat Mass Transf.* **2014**, *73*, 340–353. [\[CrossRef\]](#)
15. Sivaraj, C.; Miroshnichenko, I.V.; Sheremet, M.A. Influence of thermal radiation on thermogravitational convection in a tilted chamber having heat-producing solid body. *Int. Commun. Heat Mass Transf.* **2020**, *115*, 104611. [\[CrossRef\]](#)
16. Miroshnichenko, I.V.; Gibanov, N.S.; Sheremet, M.A. Numerical analysis of heat source surface emissivity impact on heat transfer performance in a rectangular enclosure at high Rayleigh numbers. *Int. J. Comput. Methods Eng. Sci. Mech.* **2020**, *21*, 205–214. [\[CrossRef\]](#)
17. Miroshnichenko, I.V.; Toilibayev, A.A.; Sheremet, M.A. Simulation of thermal radiation and turbulent free convection in an enclosure with a glass wall and a local heater. *Fluids* **2021**, *6*, 91. [\[CrossRef\]](#)
18. Qi, X.; Ma, W.; Liu, L. Effect of internal radiation on heat transfer during Ti:Sapphire crystal growth process by heat exchanger method. *Int. J. Heat Mass Transf.* **2021**, *170*, 121000. [\[CrossRef\]](#)
19. Parsaee, S.; Payan, S.; Payan, A. Semi-transient thermal analysis from MHD-Participating fluid into a square cavity with variable optical thickness. *Int. J. Therm. Sci.* **2021**, *169*, 107072. [\[CrossRef\]](#)
20. Gad, M.A.; Balaji, C. Effect of surface radiation on RBC in cavities heated from below. *Int. Commun. Heat Mass Transf.* **2010**, *37*, 1459–1464. [\[CrossRef\]](#)
21. Soucasse, L.; Podvin, B.; Riviere, P.; Soufiani, A. Reduced-order modelling of radiative transfer effects on Rayleigh-Benard convection in a cubic cell. *J. Fluid Mech.* **2020**, *898*, A2. [\[CrossRef\]](#)

22. Soucasse, L.; Podvin, B.; Riviere, P.; Soufiani, A. Low-order models for predicting radiative transfer effects on Rayleigh-Benard convection in a cubic cell at different Rayleigh numbers. *J. Fluid Mech.* **2021**, *917*, A5. [[CrossRef](#)]
23. Song, J.J.; Li, P.X.; Chen, L.; Li, C.H.; Li, B.W.; Huang, L.Y. A review on Rayleigh-Benard convection influenced by the complicating factors. *Int. Commun. Heat Mass Transf.* **2023**, *144*, 106784. [[CrossRef](#)]
24. Malkus, W.V.R. The Heat Transport and Spectrum of Thermal Turbulence. *Proc. R. Soc. Lond. Ser. A-Math. Phys. Sci.* **1954**, *225*, 196–212.
25. Heslot, F.; Castaing, B.; Libchaber, A. Transitions to turbulence in helium gas. *Phys. Rev. A* **1987**, *36*, 5870–5873. [[CrossRef](#)]
26. Castaing, B.; Gunaratne, G.; Heslot, F.; Kadanoff, L.; Libchaber, A.; Thomae, S.; Wu, X.Z.; Zaleski, S.; Zanetti, G. Scaling of hard thermal turbulence in Rayleigh-Benard convection. *J. Fluid Mech.* **1989**, *204*, 1–30. [[CrossRef](#)]
27. Sano, M.; Wu, X.Z.; Libchaber, A. Turbulence in helium-gas free-convection. *Phys. Rev. A* **1989**, *40*, 6421–6430. [[CrossRef](#)]
28. Shraiman, B.I.; Siggia, E.D. Heat-transport in high-Rayleigh-number convection. *Phys. Rev. A* **1990**, *42*, 3650–3653. [[CrossRef](#)]
29. Siggia, E.D. High Rayleigh number convection. *Annu. Rev. Fluid Mech.* **1994**, *26*, 137–168. [[CrossRef](#)]
30. Grossmann, S.; Lohse, D. Scaling in thermal convection: A unifying theory. *J. Fluid Mech.* **2000**, *407*, 27–56. [[CrossRef](#)]
31. Grossmann, S.; Lohse, D. Thermal convection for large Prandtl numbers. *Phys. Rev. Lett.* **2001**, *86*, 3316–3319. [[CrossRef](#)] [[PubMed](#)]
32. Grossmann, S.; Lohse, D. Prandtl and Rayleigh number dependence of the Reynolds number in turbulent thermal convection. *Phys. Rev. E* **2002**, *66*, 016305. [[CrossRef](#)] [[PubMed](#)]
33. Grossmann, S.; Lohse, D. Fluctuations in turbulent Rayleigh-Benard convection: The role of plumes. *Phys. Fluids* **2004**, *16*, 4462–4472. [[CrossRef](#)]
34. Chakraborty, S. On scaling laws in turbulent magnetohydrodynamic Rayleigh-Benard convection. *Phys. D-Nonlinear Phenom.* **2008**, *237*, 3233–3236. [[CrossRef](#)]
35. Zuerner, T.; Liu, W.; Krasnov, D.; Schumacher, J. Heat and momentum transfer for magnetoconvection in a vertical external magnetic field. *Phys. Rev. E* **2016**, *94*, 043108. [[CrossRef](#)]
36. Zurner, T. Refined mean field model of heat and momentum transfer in magnetoconvection. *Phys. Fluids* **2020**, *32*, 107101. [[CrossRef](#)]
37. Yan, M.; Tobias, S.M.; Calkins, M.A. Scaling behaviour of small-scale dynamos driven by Rayleigh-Benard convection. *J. Fluid Mech.* **2021**, *915*, A15. [[CrossRef](#)]
38. Urban, P.; Králík, T.; Hanzelka, P.; Musilova, V.; Vezník, T.; Schmoranzler, D.; Skrbek, L. Thermal radiation in Rayleigh-Benard convection experiments. *Phys. Rev. E* **2020**, *101*, 043106. [[CrossRef](#)] [[PubMed](#)]
39. Wu, X.Z.; Libchaber, A. Scaling relations in thermal turbulence—The aspect-ratio dependence. *Phys. Rev. A* **1992**, *45*, 842–845. [[CrossRef](#)]
40. Li, P.X.; Luo, X.H.; Chen, L.; Song, J.J.; Li, B.W.; Karcher, C. Numerical research for the effect of magnetic field on convective transport process of molten salt in Rayleigh-Bénard system. *Int. J. Therm. Sci.* **2024**, *195*, 108605. [[CrossRef](#)]
41. Zhang, S.; Sun, X. Convective and radiative heat transfer in molten salts. *Nucl. Technol.* **2020**, *206*, 1721–1739. [[CrossRef](#)]
42. Xie, M.; Zhu, Y.; Liu, Y.; Yuan, Y.; Tan, H. Measurement of spectral radiative characteristics of molten salt at high temperature using emission method. *Appl. Therm. Eng.* **2019**, *149*, 151–164. [[CrossRef](#)]
43. Huang, M.; Wang, Y.; Bao, Y.; He, X. Heat transport and temperature boundary-layer profiles in closed turbulent Rayleigh-Bénard convection with slippery conducting surfaces. *J. Fluid Mech.* **2022**, *943*, A2. [[CrossRef](#)]
44. Yang, J.L.; Zhang, Y.Z.; Jin, T.C.; Dong, Y.H.; Wang, B.F.; Zhou, Q. The Pr-dependence of the critical roughness height in two-dimensional turbulent Rayleigh-Bénard convection. *J. Fluid Mech.* **2021**, *911*, A52. [[CrossRef](#)]
45. Hossain, M.A.; Takhar, H.S. Thermal radiation effects on the natural convection flow over an isothermal horizontal plate. *Heat Mass Transf.* **1999**, *35*, 321–326. [[CrossRef](#)]
46. Song, J.; Li, P.; Chen, L.; Zhao, Y.; Tian, F.; Li, B. Correlations for the transport characteristics of Radiative Rayleigh-Bénard convection in optically thick media. In Proceedings of the 21st International Conference on Sustainable Energy Technologies, Shanghai, China, 12–14 August 2024.

Disclaimer/Publisher’s Note: The statements, opinions and data contained in all publications are solely those of the individual author(s) and contributor(s) and not of MDPI and/or the editor(s). MDPI and/or the editor(s) disclaim responsibility for any injury to people or property resulting from any ideas, methods, instructions or products referred to in the content.